Journal of Catalysis 414 (2022) 257–266

Contents lists available at ScienceDirect

Journal of Catalysis

journal homepage: www.elsevier.com/locate/jcat

Adsorption, thermal conversion, and catalytic hydrogenation of acrolein on Cu surfaces

Mindika Tilan Nayakasinghe [a,1], Rodrigo Ponce Perez [b], Bo Chen [a,2], Noboru Takeuchi [b], Francisco Zaera [a,*]

[a] Department of Chemistry and UCR Center for Catalysis, University of California, Riverside, CA 92521, USA
[b] Centro de Nanociencias y Nanotecnología, Universidad Nacional Autónoma de México, Apartado Postal 14, Ensenada, Baja California Código 22800, México

ARTICLE INFO

Article history:
Received 12 August 2022
Revised 13 September 2022
Accepted 15 September 2022
Available online 20 September 2022

Keywords:
Selective hydrogenation
Unsaturated alcohols
Single-atom alloy catalysis
Infrared absorption spectroscopy
Temperature programmed desorption
Density functional theory
High-pressure cell
Adsorption geometry
Reaction kinetics

ABSTRACT

The adsorption, thermal chemistry, and catalytic hydrogenation of acrolein on copper model surfaces was characterized by a combination of surface-science techniques, namely, reflection–absorption infrared spectroscopy (RAIRS) and temperature program desorption (TPD), quantum mechanics (DFT) calculations, and catalytic kinetic measurements using a so-called "high-pressure cell". Adsorption of acrolein on the Cu surface was found to involve both the carbonyl oxygen atom and the C=C bond. Thermal activation leads to early dissociation and dehydrogenation to produce acetylene and carbon monoxide below 160 K, and later to the production of ketene (220 K) and propene (260 K). Under vacuum hydrogenation with H_2 is not possible, but upon predosing of the surface with atomic H all the possible hydrogenation products, namely, propanal, 1-propanol, and allyl alcohol, were detected in TPD experiments, at 162, 190, and 210 K, respectively. Finally, catalytic hydrogenation under atmospheric pressures is slow and only produces propanal, at turnover frequencies below 0.2 s^{-1}.

1. Introduction

Hydrogenation catalysis is quite ubiquotous in the chemical industry. Many materials have been tested to promote these reactions, and yet, to date, most are catalyzed by late transition metals; Pt, Pd, and Rh are particularly efficient for these processes [1–3]. Unfortunately, those metals are not very selective, and tend to hydrogenate most if not all of the double and triple bonds in organic molecules with multiple unsaturations. In the case of unsaturated aldehydes, they usually react with the C=C bonds first, to produce saturated aldehydes (and eventually saturated alcohols) [4–8]. Many approaches have been tested to selectively hydrogenate the carbonyl group and to produce the often desirable and more valuable unsaturated alcohol instead [9–11], but the search for catalysts to perform such selective hydrogenation reactions is still ongoing.

One promising option is to use coinage metals such as copper, silver, or gold to control hydrogenation selectivity. The limitation in this case is that those metals are not able to efficiently activate molecular hydrogen [12–14], the first step required to perform most hydrogenation catalysis. It has been recently proposed that it may be possible to combine the H_2 activation functionality of metals such as Pt or Pd with the presumed selectivity in hydrogenation of Cu or Ag by using very dilute alloys of the first with the second [15–20]. In these so-called single-atom alloy (SAA) catalysts, the more active metal (Pt, Pd) is believed to be present on the surface in atomic form, and to dissociate H_2 molecules coming from the gas phase and to spill over the resulting adsorbed hydrogen atoms onto the surface of the majority alloy component (Cu, Ag) for the hydrogen incorporation steps into the organic reactants [18,21].

Empirically, it has become clear that SAA catalysts can in many instances improve the selectivity of hydrogenation reactions [22–27]. How that occurs, however, is still being debated. Much elegant surface-science work using model metal surfaces such as single crystals and controlled ultra-high vacuum (UHV) environments has been performed, mainly by the Sykes group, to support this proposed mechanism of how selective hydrogenation may work with SAA catalysts [23,28–30], and quantum mechanics calculations have complemented the experimental work [31–33]. On the other hand, evidence from our group and from others indicate that the performance of real SAA catalysts, which typically contain SAA

* Corresponding author.
E-mail address: zaera@ucr.edu (F. Zaera).
[1] Present address: Intel Corporation, Hillsboro, OR 97124, USA.
[2] Present address: Department of Pathology, Stony Brook University School of Medicine, Stony Brook, NY 11794-8691, USA.

https://doi.org/10.1016/j.jcat.2022.09.013
0021-9517/

nanoparticles dispersed on a high-surface-area oxide support, may be affected by additional factors such as the potential oxidation of the surface of the nanoparticles and/or the ease with which metals segregate to the surface or diffuse into the metal bulk upon exposure to various chemical environments [26,34–38].

In addition, the presumed selectivity of coinage metals in hydrogenation catalysis is assumed but has in general not been proven. As mentioned above, these metals do not activate molecular hydrogen, and therefore are difficult to test directly for their catalytic performance. Instead, we have embarked in a series of surface-science experiments using atomic (rather than molecular) hydrogen, complemented with density functional theory (DFT) calculations, to better understand the thermodynamics and kinetics of the adsorbed species and elementary steps associated with the hydrogenation of unsaturated aldehydes, specifically on Cu surfaces. Our previous published work showed that in the case of crotonaldehyde the molecule prefers to bind to the surface via its oxygen atom, a configuration that leads to the kinetic preference of hydrogen addition at the alpha (carbonyl) carbon position [39] and to the eventual production of the unsaturated alcohol [26]. The behavior of cinnamaldehyde was found to be more nuanced because the energetics of bonding in several configurations with different degrees of coordination to the surface are similar and affected by surface coverage [40], but even in that case Cu-Pt SAA catalysts have been shown to promote the selective hydrogenation to the corresponding unsaturated alcohol [26,27]. Here we report results from our study with acrolein. We find that with this small molecule multiple coordination to the surface may be preferred, and that, consequently, hydrogenation may occur preferentially at the C=C bond, to produce the undesirable saturated aldehyde (propanal) instead. The details follow.

2. Materials and methods

The experimental work reported here was carried out in two UHV surface-science instruments. The reflection–absorption infrared spectroscopy (RAIRS, or IRAS) and the catalytic experiments were carried out in a two-tier system described in more detail elsewhere [39,41]. The main level is used for sample cleaning, which is performed by a combination of argon ion bombardment and annealing. A UTI 100C quadrupole mass spectrometer is used for temperature programmed desorption (TPD) experiments, and here to analyze the gas mixtures during the course of the catalytic reactions performed in the high-pressure cell (see below); a computer interface affords the recording of the time evolution of the signals of up to 15 chosen amus as a function of time. A horizontal long-travel manipulator is used to resistively heat and liquid-nitrogen cool and to position the solid sample (a 10-mm-in-diameter, 1-mm-thick disk made out of oxygen-free polycrystalline copper, polished to a mirror finish) at the second level of this chamber for kinetic studies of catalytic reactions. A retractable cell (typically referred to as a "high pressure cell", or HPC; with NaCl windows to be able to perform RAIRS experiments *in situ* during catalysis) is used to isolate the solid sample and to expose it to the desired gases [42]. The cell is connected via two 1/4″ stainless-steel tubes to a close loop that acts as a well-stirred batch reactor, in an arrangement similar to that used in our lab for non-UHV experiments [43]. A side arm of the reactor's loop is connected to a leak valve attached to the UHV chamber in order to continuously monitor the gas composition in the reactor. The RAIRS setup is located in the atmospheric-pressure cell side of this two-tier instrument [44,45]: the IR beam from a Bruker Equinox 55 Fourier-transform infrared (FT-IR) spectrometer is directed through a polarizer into the inside of the UHV chamber, focused at grazing incidence onto the sample, and collected by a narrow-band mercury-cadmium-telluride (MCT) detector. The entire beam path is purged with CO_2-free and dry air. All spectra were acquired by averaging the data from 4096 scans taken at a resolution of 4 cm^{-1} and ratioed against spectra from the clean sample obtained in the same way but before gas dosing [46,47].

The TPD data were acquired in a second system equipped with a UTI 100C quadrupole mass spectrometer with an electron-impact ionizer similar to that in the first chamber, interfaced to a personal computer capable to collecting data for up to 15 different masses in a single TPD run [48,49]. An electrical interference that could not be eliminated lowered the quality of the TPD data, limiting the amount of information that could be extracted from them, so here we have restricted ourselves to reporting features that are clearly seen above the noise level and provide a statistical analysis in the case of the most relevant data (for the hydrogenation of acrolein) to add quantitative support for the identification of the main desorption peaks (Table 2). This second UHV instrument also has a 50-mm radius hemispherical electron energy analyzer (VSW HAC 5000) and an aluminum-anode (hν = 1486.6 eV) X-ray source to perform XPS experiments, to check on the cleanliness of the surface, and a rasterable ion gun (Perkin-Elmer PHI 04–300) for sample cleaning (using 2 kV Ar^+ ions followed by annealing at 1100 K) [48,50]. The 10-mm-in-diameter, 1-mm-thick polished Cu(1 1 0) single crystal was mounted on an on-axis manipulator capable of x-y-z-θ motion and of resistive heating and liquid-nitrogen cooling [51].

The temperature of both the polycrystalline and the single-crystal copper surfaces was followed by using K-type thermocouples wedged into a hole drilled on the side of the solid samples, and controlled by homemade proportional-integral-derivative (PID) circuits; a constant heating rate of 5 K/s was used in the TPD experiments. For the experiments on oxidized samples, the surfaces were exposed to 30 L of O_2 (Liquid Carbonic, Research Purity, >99.995 %) at 500 K prior to the adsorption of the unsaturated aldehyde, a treatment that yields a surface coverage of $\theta_O \sim 0.4$ ML in an incomplete (2 × 1) structure [40,52–54]. Pre-saturation of the surface with atomic hydrogen was accomplished by flowing H_2 (1×10^{-5} Torr × 300 s; Airgas, >99.99 % purity) through a hot W filament (resistively heated with 11 V × 14 A ∼ 150 W power) placed in front of the Cu(1 1 0) crystal, about 5 cm away [14]. Dosing of the samples was done by backfilling of the chamber using leak valves, and is reported in Langmuirs ($1\ L = 1 \times 10^{-6}$ Torr s), uncorrected for differences in ion gauge sensitivities. The pressure in the main UHV chamber was measured by using a nude ion gauge. Acrolein was purchased from Aldrich (>90 purity), purified *in situ* by performing several freeze–pumpthaw cycles, and introduced into either the UHV chambers or the catalytic batch reactor using its vapor (and leak valves in the UHV cases).

The raw TPD and kinetic data were deconvoluted and calibrated using a protocol developed in our laboratory to convert mass spectrometer signals into partial pressures for the different reactants and products [55–57]. The signals for 56, 57, 58, and either 59 or 31 amu (59 amu for the TPD, 31 amu for the catalytic kinetics) were selected for these calculations, as they are important peaks in the mass spectra of acrolein (2-propenal), allyl alcohol (2-propenol), propanal, and 1-propanol, respectively; these are the main reactants and products expected from acrolein hydrogenation. The kinetic data were converted into turnover numbers (TON, in units of number of organic molecules per copper surface atom) using an independent mass-spectrometer signal calibration into gas pressures, the volume of the reactor, and the surface area of the Cu surface; turnover frequencies (TOF) were then calculated by numerical derivatization of the TON-versus-time plots, and reported in units of TON/s [56]. The reported error bars were estimated from the standard deviations around the averages of several runs carried out under identical conditions.

DFT calculations were performed using the Vienna *Ab initio* Simulation Package (VASP),[58] with projector augmented waves [59]. The exchange–correlation energies have been treated according to the generalized gradient (GGA) approximation with Perdew–Burke–Ernzerhof (PBE) parametrization [60], and Van der Waals forces have been considered employing the GrimmeD3 correction method [61]. The one-electron states have been expanded using the projector-augmented wave basis (PAW) [59], with an energy cutoff of 400 eV. Surface cells were composed of a slab formed by 4 monolayers and a vacuum space of 25 Å. Both (2 × 2) and (3 × 3) periodicities in the x-y plane were used, which we associate with high (θ_{high} = 1/4 ML; ML = monolayer) and low (θ_{low} = 1/9 ML) coverages, respectively. The Brillouin zone has been sampled with k-point grids of 5 × 5 × 1 and 3 × 3 × 1 for the (2 × 2) and (3 × 3) surface unit cells, respectively, employing the Monkhorst-Pack scheme. Reaction pathways and activation energies were calculated by using the nudged elastic band (NEB) method [62,63] within the climbing image scheme, as implemented in VASP.

3. Results

3.1. Adsorption

We start our discussion of the characterization of the thermal chemistry of acrolein on copper surfaces by exploring its adsorption mode using a combination of RAIRS data and DFT quantum mechanics calculations. The RAIRS sequences for the uptake of acrolein at 90 K on both clean (left) and oxygen predosed (right) polycrystalline Cu surfaces are shown in Fig. 1, and their peak assignments are provided in Table 1. On the clean Cu, only one main peak is clearly seen, at 1650 cm^{-1}, for exposures below 5 L, which was determined to be the dose needed to achieve monolayer saturation; we identify this feature as originating from the C═O stretching mode (νC = O)). The peak is red-shifted from its 1684 cm^{-1} value in solid acrolein, an indication that there is a direct interaction between the carbonyl group and the surface. Moreover, its relatively high intensity suggests that the C═O bond is oriented at an angle from the surface plane (based on the surface selection rule that applies to RAIRS on metal surfaces [47,64]). Additional weaker features can be observed in the 5 L spectrum as well, at approximately 986, 1176, and 1427 cm^{-1}, corresponding to methylene wagging ($\omega(CH_2)$), carbon–carbon single-bond stretching (ν(C—C)), and methylene scissoring ($\gamma(CH_2)$) modes, respectively. Conspicuously absent is the peak for the stretching of the C═C double bond, a result that may be interpreted as being the consequence of having such bond lying parallel to the surface (although this is not conclusive, since the feature shows a low intensity even in the IR of the pure solid). A rehybridization of the C═C bond, typical in the adsorption of unsaturated carbon–carbon bonds on metals [8,65,66], can explain why both the wagging and scissoring modes of the methylene moiety are seen (implying that its plane must not be parallel to the surface), and also why the C—C single bond (next to the carbonyl moiety) is detectable in the RAIRS as well.

Exposures larger than 5 L lead to the condensation of acrolein on the surface. This is clearly manifested by the growth of the new peaks at 1165 (ν(C—C), slightly red-shifted from the value in the monolayer), 1365 ($\delta_{ip}(CH)_{ald}$, an in-plane deformation motion of the aldehyde hydrogen atom), 1426 ($\gamma(CH_2)$, now sharp), 1610 (ν(C═C), weak but observable), and 1697 (ν(C═O)) cm^{-1}. Adsorption on oxygen pre-treated surfaces follows approximately the same sequence of events, except that in the acrolein monolayer the $\gamma(CH_2)$ is less visible and a weak signal at 1350 cm^{-1} is seen for the $\delta_{ip}(CH)_{ald}$ mode instead. This suggest a new adsorption geometry with less C═C rehybridization and an aldehyde group oriented at more of an angle from the surface plane.

The structure of the adsorbed acrolein was estimated using quantum-mechanics DFT calculations. Fig. 2 summarizes the results for the optimized adsorption energies of several binding

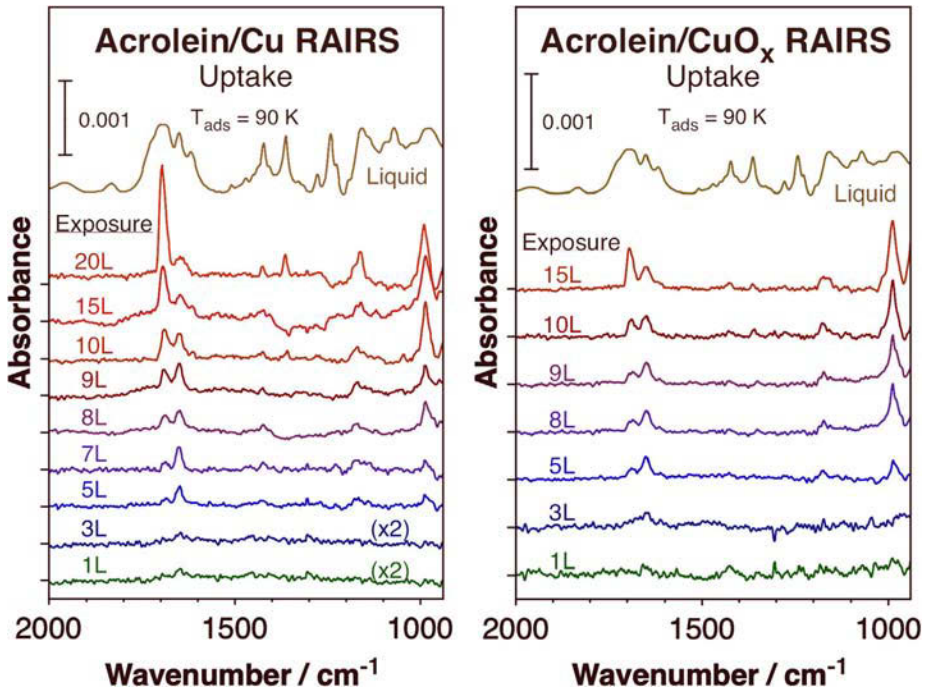

Fig. 1. RAIRS of acrolein adsorbed on clean (left) and oxygen-pretreated (right) polycrystalline copper surfaces at 90 K. Data are provided as a function of acrolein dose. The spectrum of liquid acrolein is provided at the top for comparison.

Table 1
Peak assignment of the peaks in the RAIRS data in Fig. 1, for acrolein adsorbed on clean and oxygen-predosed Cu surfaces. Data for pure liquid acrolein and for acrolein condensed on Pt(111) are also provided as references.

Mode[a]	8L Acrolein/Cu	8L Acrolein/O/Cu	Acrolein, Solid[b]	Condensed, Pt(111)[c]
$\omega(CH_2)$	986 (s)	989 (s)	993 (s)	993 (s)
ν(C—C)	1176 (m)	1174 (m)	1159 (m), 1161 (m)	1166 (m)
$\delta_{ip}(CH)_{ald}$		1350 (w)	1365 (m)	1367 (m)
$\gamma(CH_2)$	1427 (w)		1425 (w)	1427 (w)
ν(C=C)	1610 (w)	1612 (w)	1618 (w)	1618 (w)
ν(C=O)	1650 (s)	1650 (s)		
ν(C=O)	1697 (s)	1693 (s)	1684 (s)	1662 (m), 1700 (s)

[a] ω = wagging, ν = stretching, δ = deformation, γ = scissoring, ip = in-plane, ald = aldehyde, s = strong, m = medium, w = weak.
[b] Ref[67].
[c] Ref[68].

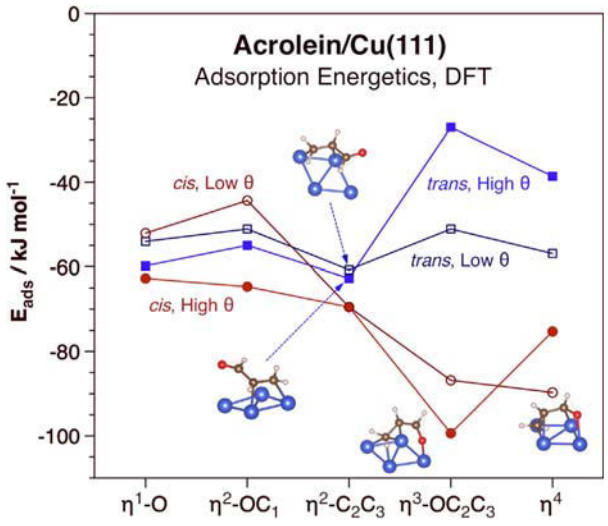

Fig. 2. DFT-calculated energies for different adsorption modes of acrolein on a Cu(111) surface. Shown are values for 5 types of coordination, going from a single bond to the oxygen atom (η^1-O) to full coordination to all three carbons and the oxygen atom (η^4). Also provided are values for both *cis* and *trans* isomers of acrolein, and for adsorption on a small ((2×2)) and on a larger ((3×3)) unit cell, representing surface coverages of θ = 1/4 (high) and θ = 1/9 (low) monolayers, respectively. The structures of the most stable structures are shown as well (other structures are provided in Fig. S1, Supporting Information).

configurations with increasing number of coordination atoms, transitioning (from left to right in Fig. 2) from a single bond to the oxygen atom (η^1-O) to full coordination to all three carbons and the oxygen atom (η^4). Both *cis* and *trans* isomers were considered, and values for two surface coverages, labeled "low" (θ = 1/9, calculated using a (3×3) unit cell) and "high" (θ = 1/4, employing a (2×2) unit cell), are reported. Several lessons are easily extracted from these data. For one, it is clear that adsorption in the *cis* configuration is more stable than in the *trans* counterpart. It is also noticeable that multiple coordination generally stabilizes the *cis* isomer but destabilizes the *trans* isomer. In the end, the most stable coordinations to the surface were determined to be the η^4 and η^3-OC_3C_4 bondings at low and high coverages, respectively, both in *cis* configurations. The structures of these adsorbates, also shown in Fig. 2, are consistent with the RAIRS data, in that bonding to the surface involves a strong interaction with the oxygen atom (leading to the rehybridization responsible for the red shift of the ν(C=O) peak) and additional coordination of the C=C bond with its axis parallel to the surface. In this arrangement, the C—C single bond is at an angle from the surface plane, and so is the aldehyde plane; hence their detection in the vibrational data. The structures of the other bonding modes are reported in Fig. S1 (Supporting Information).

3.2. Thermal reactivity

The thermal chemistry of acrolein adsorbed on a Cu(110) single crystal surface was characterized by TPD. Multiple experiments were carried out to cover a wide range of values of amus, to help identify the relevant desorption products, and also as a function of exposure. Fig. 3 displays key traces in the 14 to 31 amu range after adsorption of 3, 7, 11, 15, and 20 L acrolein at 85 K. It is seen there that, at all coverages, peaks are only seen for 26, 27, 28, and 29 amu, with maximum signal about 170 K. Most of those signal are associated with molecular acrolein desorption, but there is an excess contribution in the 26 amu trace in the low-temperature side, around 160 K, which we identify as coming from acetylene; this is the most obvious in the low-dose spectra (first two panels of Fig. 3). The 28 amu spectrum also displays excess intensity in its low-temperature end, around 150 K, coming from the production of carbon monoxide; it appears that some of the adsorbed acrolein undergoes a scission reaction at the C—C single bond, followed by dehydrogenation to produce CO and HC≡CH. Furthermore, there is some excess signal in the 27 amu trace originating from propene, as discussed next. On the other hand, the absence of any signal for 30 amu rules out the formation and desorption of any formaldehyde.

The left panel of Fig. 4 reports the corresponding TPD traces in the 37 to 41 amu range from a Cu(110) surface dosed with 15 L acrolein. Clear peaks are seen around 260 K in the 39, 41, and 42 amu traces, with approximately 0.9:1.0:0.6 area ratios, as expected for propene. The 42 amu trace does peak at a lower temperature, at about 220 K, and shows additional intensity likely coming from ketene. This additional chemistry yielding propene and ketene does take place at higher temperatures than that required for simple splitting of the molecule into CO and acetylene, and most likely represents a parallel decomposition pathway. In terms of the potential production of water, none is seen on the clean Cu(110) (the center panel of Fig. 4 does not show any discernible signal in the 18 amu trace), but some water is produced if the surface is predosed with oxygen (Fig. 4, right panel), in two stages at around 420 and 470 K. It is likely that the coadsorbed oxygen atoms help with hydrogen extraction steps, to form surface OH (ads) intermediates and ultimately H_2O.

3.3. Acrolein hydrogenation

The TPD data in the 39–60 amu range for 7 L acrolein adsorbed on Cu(110) are summarized in Fig. 5. On the clean Cu(110) surface (left panel), the main signals are seen in the 55 and 56 amu traces, which show peaks at approximately 170 K, skewed toward the high-temperature side; these correspond to acrolein molecular desorption. Moreover, a second sharp feature starts to grow at 165 K after exposures > 7 L due to multilayer condensation (a small feature is already seen in the traces in Fig. 5). Broad and weak fea-

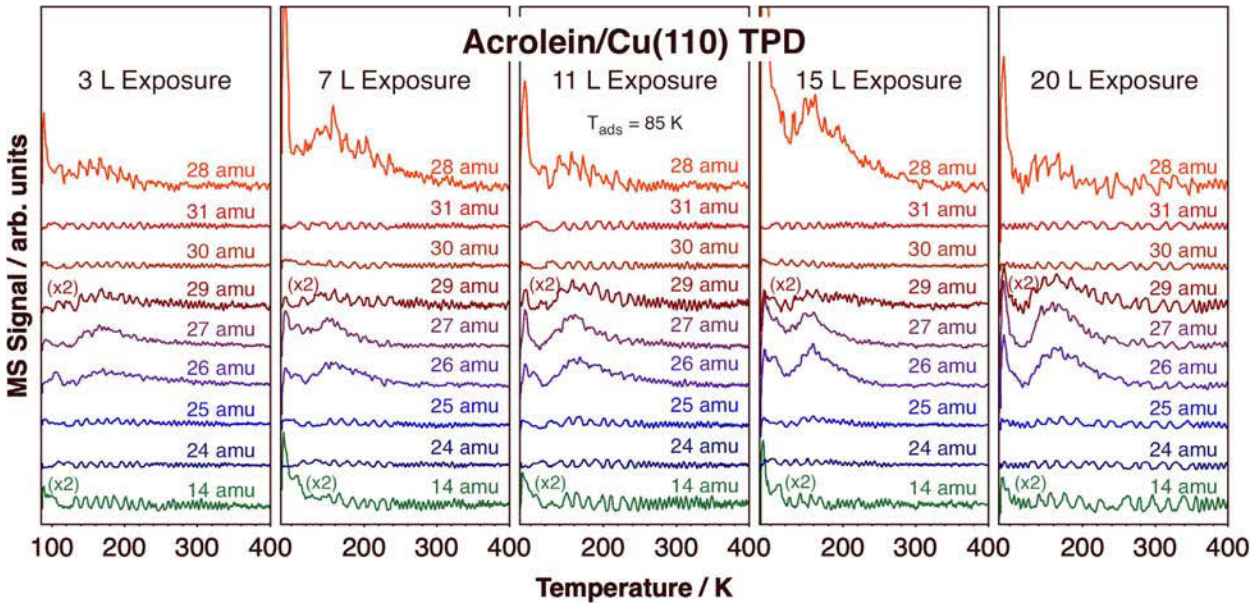

Fig. 3. TPD traces from acrolein adsorbed on a Cu(1 1 0) surface. The five panels correspond to data obtained for increasing surface coverages, after 3, 7, 11, 15, and 20 L doses, all at a surface temperature of 85 K. Each panel reports traces for, from bottom to top, 14, 24, 25, 26, 27, 29, 30, 31, and 28 amu.

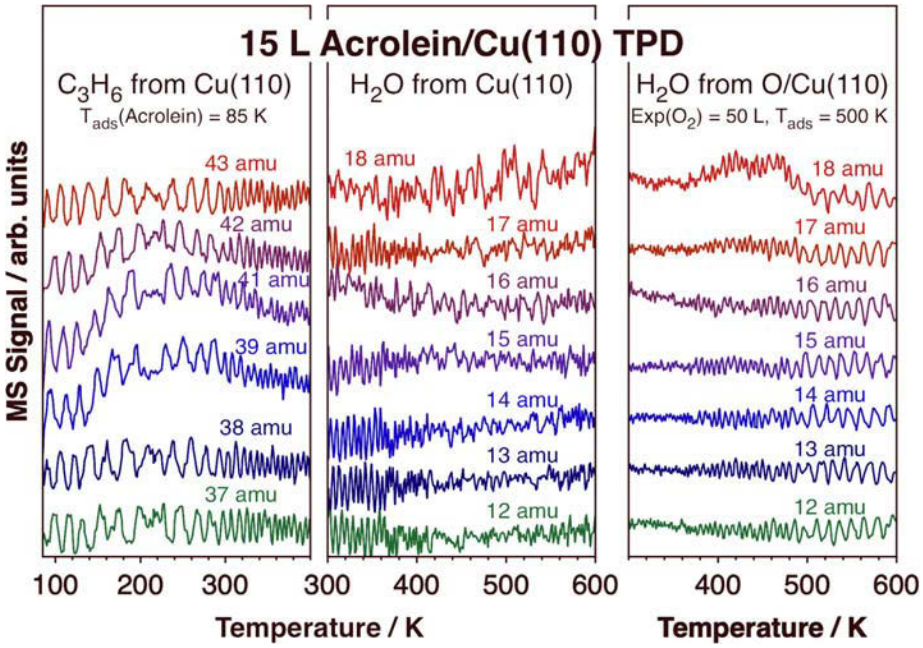

Fig. 4. TPD data from 15 L acrolein adsorbed on a Cu(1 1 0) surface at 85 K. Left: Traces for 37, 38, 39, 41, 42, and 43 amu, used to identify propene. Center: Traces for 12, 13, 14, 15, 16, 17 and 18 amu, used to probe the possible formation of water. Right: similar set of data to that in the center panel but for experiments on a Cu(1 1 0) surface pretreated with O_2 (50 L, 500 K).

tures are seen in the 57 and 58 traces, starting at 185 K, indicating that some minor hydrogenation may take place in this case, likely via the incorporation of surface hydrogen atoms generated by the decomposition of some of the acrolein molecules discussed above. Pretreating the surface with oxygen inhibits this hydrogenation pathways, and enhances the yields for molecular desorption (Fig. 5, second-from-left panel). Predosing molecular hydrogen also results in acrolein molecular desorption only, without any hydrogenation; H_2 does not adsorb on copper surfaces under the conditions of the experiment [12–14]. On the other hand, predosing the Cu(1 1 0) substrate with atomic hydrogen opens a number of hydrogenation reaction channels: detectable signals are seen in the 57 to 60 amu traces of the TPD in this case (Fig. 5, second-from-right panel). In fact, it is clear that several hydrogenation products are made, because different peaks with different shapes are seen in each of those four traces. This becomes clearer once the data are deconvoluted into the different potential products (following the analysis mentioned and referenced in the Materials and Methods section), as shown in the far-right panel of Fig. 5. In spite of the large noise associated with these data, all three hydro-

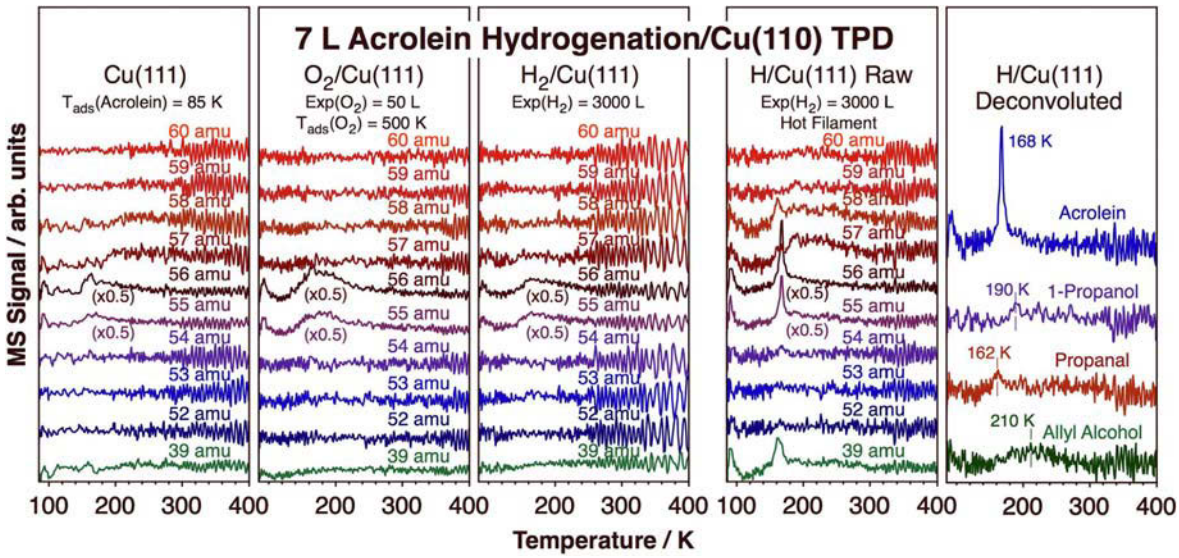

Fig. 5. TPD traces in the 39–60 amu range from 7 L acrolein dosed on Cu(1 1 0) surfaces at 85 K. Left: Adsorption on the clean surface. Second-from-left: Adsorption on a oxygen pretreated (50 L O_2 at 500 K) surface. Center: Adsorption on a surface predosed with 3000 L H_2. Second-from-right: Adsorbed on a surface predosed with atomic hydrogen (3000 L H_2 dose through a hot filament). Right: Deconvoluted spectra for the atomic-hydrogen predosing case.

Table 2
Summary of data from a statistical analysis of the TPD for 7 L acrolein adsorbed on a Cu(1 1 0) surface predosed with atomic hydrogen (Fig. 5, right panel).

Compound	Peak T / K	Peak Range / K	Peak Area / V K	RMS × ΔT / V K
Acrolein	168	150–200	35.2	7.7
Propanal	162	150–180	8.9	4.1
1-Propanol	190	170–220	9.3	4.6
Allyl Alcohol	210	160–260	25.9	5.4

genation products are seen: propanal, in a peak at 162 K, 1-propanol, at 190 K, and allyl alcohol (1-propenal), in a broad feature centered around 210 K. To make sure that the reported features are real, a statistical analysis was carried out to compare the areas under these peaks against the areas expected on flat traces with equivalent levels of RMS (root mean square) noise; The resulting numbers, summarized in Table 2, show that all the reported peaks are at least a factor of two larger than the area from the baseline, clearly above the noise. Significantly, propanal appears to be the most energetically favorable product, as it desorbs at the lowest temperature, whereas allyl alcohol seems to be the least (although it shows the highest yield, about 25 % of all desorption). This trend is opposite to that seen with other unsaturated aldehydes [14,26], and suggests that Cu-based catalyst may not promote acrolein hydrogenation with the desired selectivity toward the unsaturated alcohol. We address this point in more detail below.

To better understand the selectivity observed in the TPD traces for the hydrogenation products in the case of coadsorbed acrolein and atomic hydrogen, DFT calculations were performed to estimate the adsorption energies and configurations of the likely intermediates and the activation barriers for the hydrogenation steps. First, all possible optimized structures were calculated for adsorbed acrolein after the addition of either one or two hydrogen atoms: the results, starting from the η^4-*cis* and η^2-C_2C_3-*trans* acrolein structures on the (3 × 3) unit cell, are provided in Figs. S2 and S3, respectively (Supporting Information). In both cases, addition at the C_γ position (that is, the carbon farthest from the oxygen atom) is the step that yields the most stable monoprotonated species (mH_4 in our nomenclature, where m stands for "mono", that is, one single H addition, and the number 4 corresponds to the 4th atom counting from the O end); protonation at the C_α position (mH_2) is a distant second preference. For the *cis* isomer, the most energetically favorable place to add the second hydrogen atom is at the C_β position, to produce adsorbed propanal ($dH_{3,4}$ in our nomenclature with d standing for "di", that is, for the addition of two hydrogen atoms). With the *trans* isomer, the second H addition is preferred at the O atom instead, to produce an enol species (1-propenol, or $dH_{1,4}$ in our nomenclature). However, in both cases the adsorption energies of the propanal ($dH_{3,4}$) and 1-propenol ($dH_{1,4}$) are quite close, within the error of the calculations, so it is difficult to determine which species would be the one that is preferentially produced. 2-propenol (allyl alcohol, $dH_{1,2}$), by contrast, is 30–35 kJ/mol less stable on the Cu(1 1 1) surface than either of the other two structures.

A similar trend in terms of adsorption stability was reported by us already for the adsorption of crotonaldehyde on Cu(1 1 1): the most stable products from the hydrogenation of crotonaldehyde are also the mH_4 and $dH_{3,4}$ (butanal) adsorbed species [26]. However, in that case it was determined that selectivity toward the production of the unsaturated alcohol, as seen experimentally, is due to a kinetic control because of the high barrier for the addition of H atoms to the C=C bond in the adsorbed unsaturated aldehyde. A similar determination of the potential energy pathways for the different possible hydrogenation reactions was made here for acrolein on Cu(1 1 1). In Fig. 6 the results from calculations starting with the η^4-bonded *cis* isomer on a (3 × 3) Cu(1 1 1) unit cell, the most stable species identified in our calculations at low coverages, are shown. It can be clearly see there that in this case the path with the lowest activation barrier is the incorporation of a H atom

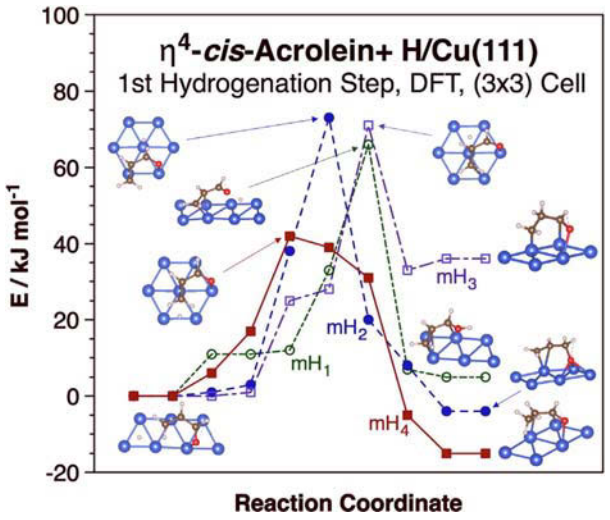

Fig. 6. DFT-calculated potential energy pathways for the incorporation of the first hydrogen atom to η^4-*cis*-acrolein adsorbed on a Cu(1 1 1) surface (using a (3 × 3) unit cell). Shown are the optimized routes for the addition to the four possible positions, to the oxygen atom and to each of the three carbons (nomenclature: mH_x, where m stands for "mono" indicating the addition of only one hydrogen atom, and x indicates the addition position: 1 = O, 2 = C_α, 3 = C_β, and 4 = C_γ). Also provided are the structures of the transition states and the final adsorbed species. The starting point in all cases is the Cu(1 1 1) surface with coadsorbed acrolein plus one hydrogen atom.

into the C_γ position (mH_4); whereas the activation energies for that path is approximately 40 kJ/mol, the barrier for the three other reactions range from 66 kJ/mol (to produce mH_1) to 73 kJ/mol (mH_2; the barrier for mH_3 is 71 kJ/mol).

The energetics of the reaction coordinates of other possible hydrogenation pathways for the most stable acrolein species adsorbed at low ((3 × 3) cell) and high ((2 × 2) cell) coverages, in the η^4-cis and η^3-OC_2C_3 configurations, respectively, are reported in Figs. S4 and S5 (Supporting Information). The energies are referenced to a system with both acrolein and two hydrogen atoms adsorbed on Cu(1 1 1) far away from each other; a small amount of energy, on the order of 10 kJ/mol, is required for the H(ads) atoms to diffuse to positions close to the acrolein so reactions between the two species can take place, but inclusion of that step just displaces the energy scale for all cases and does not modify the trends observed in the data. As already shown in Fig. 6, Fig. S4 indicates that at low coverages the first H atom is added to the C atom farthest from the O atom, to produce the mH_4 intermediate. It can also be seen there that the second H incorporation requires less energy, and can produce either propanal (the $dH_{4,3}$ pathway) or 1-propenal (an enol intermediate, the $dH_{4,1}$ route); the energy difference between the two activation barriers is small, less than 10 kJ/mol. At high coverages (Fig. S5, Supporting Information), H addition at the C_β atoms may be the most favorable, but the resulting intermediate (mH_3) is likely to be a dead end. Instead, the $dH_{4,3}$ and $dH_{4,1}$ are likely to be the most feasible reaction routes: the activation barrier for the first H addition (mH_4) is 77 kJ/mol, only 12 kJ/mol larger than that for the mH_3 pathway, and the activation energy values for the second step are 39 ($dH_{4,1}$) and 44 ($dH_{4,3}$) kJ/mol, with a small but negligible preference for the formation of the enol.

Comparison between these energy values calculated using DFT and the experimental TPD data is in principle possible but needs to be done with caution. Generally, the peak temperatures in TPD can be used to estimate activation barriers [69–71], but some assumptions need to be made. In our case, things are complicated by the fact that the hydrogenation steps are second order and depend on the coverages of both acrolein (or the first hydrogenated intermediate if the second step is rate limiting) and atomic hydrogen. To simplify the calculations, here we assume that the Cu(1 1 0) surface is saturated with H ($\theta_H \sim 1$ ML) and that the kinetics follows a pseudo-first order dependence on the coverage of acrolein. Next, an adequate value for the pre-exponential factor needs to be guessed. When dealing with molecular desorption, high values, on the order of 1×10^{15} to 1×10^{19} s^{-1}, are typical, but because these hydrogenation reactions are in reality second order, a lower value needs to be used. For propanal production, a pre-exponential factor of 1×10^{13} s^{-1} yields an estimated barrier of 40 kJ/mol, in line with the low-coverage ($\theta_{acrolein}$ = 1/9 ML) activation energy calculated by DFT. The higher desorption temperatures for allyl alcohol and 1-propanol can then be explained by higher barriers for the incorporation of the third and/or fourth hydrogen atoms into the enol surface intermediate predicted by DFT. In the end, though, the most that can be safely said from this discussion is that the DFT calculations are consistent with the experimental results.

Finally, catalytic experiments were carried with the polycrystalline Cu polished disk using the high-pressure cell described in the Materials and Methods section. Typical kinetic data, in the form of turnover numbers (TON) versus time for the consumption of acrolein and for the production of the different products, are shown in Fig. 7. Two runs are reported there, for acrolein partial pressures of 2 (left panel) and 4 (right) Torr, both mixed with 300 Torr H_2; the catalysis was carried out at 490 K. A fast transient was observed within the first 5 s of starting the reaction, leading to the apparent consumption of significant amounts of acrolein and the production of both allyl alcohol and propanal. Most likely, this is an experimental artifact, or perhaps catalysis occurring rapidly on particularly active sites that get rapidly deactivated. Almost undetectable steady-state catalytic activity is seen afterwards, as expected because of the poor performance of copper for the activation of H_2. There does seem to be a slow production of propanal, however, more noticeable for the 4 Torr acrolein case; a turnover frequency (TOF) of 0.18 s^{-1} was estimated in that case. This value is orders of magnitude lower to that seen in typical hydrogenation catalysis with platinum model and real catalysts [2,42,72–75]. In any case, it also indicates that selectivity is directed toward the production of the saturated aldehyde, not the unsaturated alcohol as desired.

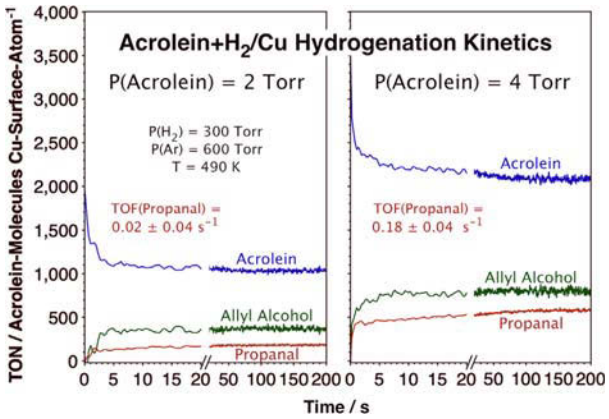

Fig. 7. Kinetics of the catalytic hydrogenation of acrolein promoted by a polished polycrystalline Cu disk, measured using a "high-pressure cell" surface-science apparatus. Data are provided for two cases, with 2 (left panel) and 4 (right) Torr acrolein mixed with 300 Torr H_2 and topped off with 600 Torr Ar, for reactions run at 490 K. The data were acquired using a mass spectrometer, and deconvoluted as explained in the Materials and Methods section to estimate the temporal evolution of the partial pressures of the reactant (acrolein) and of the different products (propanal and allyl alcohol), in units of TON. The TOFs for propanal, calculated via numerical derivatization of these plots, are reported as well.

4. Discussion

As stated in the Introduction, the main goal of this work has been to characterize the adsorption and thermal reactivity of acrolein on copper surfaces with the aim to put that knowledge in perspective and to understand the potential ability of copper-based catalysts to promote hydrogenation reactions selectively. The research was divided in several parts, starting with a study of the adsorption of acrolein. The RAIRS data obtained for the uptake of acrolein on a Cu polished polycrystalline surface clearly indicate a strong interaction of the carbonyl group, most likely via the oxygen atom, with the metal, leading to a significant rehybridization of the C═O bond and to a red shift in the frequency of the stretching frequency of that bond. The high intensity of the corresponding IR peak also suggests that the C═O bond is likely not oriented parallel to the surface plane. In addition, the lack of a peak for the stretching vibration of the C═C bond suggests a possible flat orientation for that moiety. This behavior appears to be common for unsaturated aldehydes on metal surfaces. The adsorption of acrolein has so far been characterized by RAIRS on Pt(111) [68,76,77], Ru(001) [78], Pd(111) [79,80], Ag(111) [81], and Au (111) [82], as well as on Ag [67] and Au [82] films, and in most the C═C bond seems to be oriented parallel to the surface, at least at low coverages.

Similar results were also reported by us in the past in connection with the adsorption of crotonaldehyde [26,39], and DFT calculation for cinnamaldehyde indicated a preference for binding via the oxygen atom as well [40]. It would therefore be tempting to conclude that the behavior of unsaturated aldehydes on copper surfaces occurs mainly via an interaction of the carbonyl group with the substrate, and that the C═C double bond orients itself parallel to the surface plane but does not participate in its thermal chemistry. However, the results from our DFT calculations with acrolein, reported above, highlight significant differences when compared with the previous reported results involving other molecules, and point to the uniqueness of acrolein as a surface species. In particular, Fig. 2 shows that the acrolein always prefers to adopt a *cis* configuration, like cinnamaldehyde [40] but in contrast with crotonaldehyde, where the *trans* isomer sometimes dominates [39]. Also, acrolein appears to exhibit multiple coordination to the surface involving both C═C and C═O bonds.

This new coordination is perhaps the reason why acrolein adsorbed on copper shows high thermal activity. Specifically, the TPD data in Figs. 3 and 4 show an ease for the scission of the C—C single bond, to produce acetylene and carbon monoxide at temperatures as low as 150 to 160 K, and additional conversion to ketene (220 K) and propene (260 K) at higher temperatures. Dehydrogenation steps are also manifested by the detection of small amounts of self-hydrogenation (Fig. 5, left panel). It is worth noticing that these activation steps, in particular the decarbonylation reaction, take place at quite low temperatures. It could be that they occur on defect sites on the surface. However, given that the yields are significant, they may also be explained by the open nature of the Cu(110) surface, which displays a large fraction of low-coordination Cu sites. One possible explanation here is that the multiple coordination bonding of acrolein may involve Cu atoms at both the top and trough rows of the Cu(110) plane. In future studies, we plan to compare the adsorption of acrolein on such open surface to that on Cu(111) to identify any potential differences that may explain the high reactivity seen here.

We also tested the possibility of enhancing the reactivity of the Cu surface by adding atomic oxygen, given that for other oxygenates such treatment has been shown to enhance hydrogen extraction steps [83], and because hydrogenation catalysis with copper-based SAA catalysts may take place on partially oxidized surfaces [26]. However, not much difference in the surface chemistry of acrolein was observed here between the clean and oxygen-predosed surfaces: if anything, there is less decomposition and more molecular desorption in the latter case (Fig. 4, right panel), and the self-hydrogenation steps are blocked at the expense of water formation (Fig. 5, left two panels).

Next, we discuss the possible promotion of hydrogenation reactions by Cu surfaces. Under UHV, the TPD experiments reported in Fig. 5 indicate that it is difficult to make adsorbed acrolein react with molecular hydrogen (Fig. 5, center), and that atomic hydrogen has to be supplied to test any reactivity. On the other hand, the two right panels of Fig. 5 show that, when this is done, hydrogenation products can be clearly detected. It is interesting that all three possible hydrogenation products are seen, namely, propanal (at 162 K), 1-propanol (at 190 K), and allyl alcohol (in a broad temperature range centered around 210 K). Again, this contrasts with the behavior of other unsaturated aldehydes: with cinnamaldehyde, about two thirds of the molecules that react form the unsaturated alcohol and the rest the fully hydrogenated alcohol, and saturated aldehyde production is restricted to a few percent yield [14]. No such selectivity was identified here with acrolein.

A straightforward explanation for the different behavior of acrolein in these systems is provided by the calculations summarized in Figs. S2 to S5 (Supporting Information) and in Fig. 6. In all the cases studied to date the species produced by hydrogenating the C═C bond (saturated aldehydes) are more stable than those resulting from C═O hydrogenation (unsaturated alcohols), but with crotonaldehyde, for instance, adsorption is via the oxygen atom of the carbonyl group and the C═C bond is too far from the surface to be reactive: the C═O bond hydrogenates first because the activation barrier to add the first H atom to the C═C bond is much higher [26]. With acrolein, by contrast, adsorption involves the C═C bond, and H addition to the end carbon atom is the most facile hydrogenation step (Fig. 6). The story is somewhat more nuanced, however, because all three products were detected in the TPD experiments. One possible explanation may have to do with the energetics of the second hydrogenation step, since the incorporation of a second H atom into the half-hydrogenated mH_4 surfaces species at the C_β atom or at the oxygen end produce surface species (propanal and 1-propenol, respectively) with similar activation barriers and adsorption energies (Figs. S2 to S5, Supporting Information). It could be argued that if some enol species is formed on the surface, that intermediate could then undergo a number of isomerization and hydrogenation steps to produce not only allyl alcohol (1-propenol) but also 1-propanol. It is relevant to mention here that a similar argument was put forward by us to justify why 1-butanol is a primary product during the hydrogenation of crotonaldehyde on Pt(111), as determined in molecular beam experiments [84].

Finally, we briefly discuss the results from the catalytic experiments reported in Fig. 7. Ignoring the initial jump in the concentrations of the allyl alcohol and propanal products, which is likely to come from experimental artifacts, it is seen that the polished polycrystalline Cu surface used here is quite inefficient at sustaining catalytic hydrogenation reactions. Only a small amount of propanal seems to be produced, and this at rates orders of magnitude lower than those seen with other transition metals. Moreover, propanal is the undesirable product; if a second metal where to be added in small amounts to help activate molecular hydrogen, as it is presumed to happen with SAA catalysts, chances are that the resulting catalysis would not be selective for the production of the desirable allyl alcohol. This hypothesis needs to be tested still, though.

5. Conclusions

It was found here that the adsorption of acrolein on Cu surfaces involves bonding through the carbonyl oxygen atom: the C═O stretching frequency shifts down by approximately 50 cm^{-1}, indicating rehybridization and weakening of that bond. On the other hand, the signal for the C═C stretching frequency is not detectable by RAIRS, suggesting adsorption with that bond oriented parallel to the surface. DFT calculations corroborate this interpretation, and indicate that the molecule prefers to adopt a *cis* configuration and multiple coordination to the metal: an η^4 mode was found to be the most stable at low surface coverages, and a η^3-OC_2C_3 mode the preferred one as the coverage is increased.

Thermal activation of acrolein adsorbed on a Cu(1 1 0) single-crystal surface during TPD experiments leads to some dissociation, first to yield carbon monoxide and acetylene, which desorb at 150 and 160 K, respectively, and later to produce ketene, at 220 K, and propylene, at 260 K. Most of the adsorbed acrolein desorbs molecularly, however, and a small fraction undergoes self-hydrogenation with the atomic surface hydrogen released by the dehydrogenation steps that produce the CO and acetylene. Preadsorption of oxygen on the surface blocks this latter pathway by scavenging the H atoms to produce water, at 420 and 470 K.

Pre-exposure of the surface to molecular hydrogen does not alter this chemistry in any significant way, given that copper surfaces are not efficient at activating the H—H bond and therefore do not uptake hydrogen. Predosing with atomic hydrogen generated in the gas phase, by contrast, does result in the promotion of hydrogenation reactions. All three main expected products are seen in the TPD in this case, namely, propanal (at 162 K), 1-propanol (at 190 K), and allyl alcohol (in a broad feature centered around 210 K). The preference for the formation of the saturated aldehyde, typically the undesirable product and not the one seen with crotonaldehyde, is justified by the low activation energy for the incorporation of the first hydrogen into the carbon atom farthest from the oxygen (C_γ), approximately 40 kJ/mol according to DFT calculations; the barriers for hydrogen addition to any of the other atoms in acrolein are on the order of 70 kJ/mol. On the other hand, although the energetically preferred species resulting from the addition of two H atoms to acrolein on Cu(1 1 1) is adsorbed propanal, an enol intermediate (1-propenol) is almost as viable, and could form and further isomerize at higher temperatures to yield the other two products.

Finally, polycrystalline Cu surfaces do not promote much hydrogenation catalysis. The conversion of acrolein with such catalysts under atmospheric pressures is quite slow, almost under the detectability of the instrumentation used here. With 2 Torr acrolein (and 300 Torr H_2, at 490 K), the reaction turnover frequency measured is within our experimental error, but with 4 Torr acrolein a steady-state TOF of approximately 0.2 s^{-1} was estimated. Unfortunately, the only product detected was propanal. It appears that, with acrolein, copper does not promote the desired selective hydrogenation to the unsaturated alcohol, and may therefore not be a good choice to use in single-atom alloy (SAA) catalysts for this purpose. In this, acrolein behaves differently than crotonaldehyde.

Data availability

Data will be made available on request.

Declaration of Competing Interest

The authors declare that they have no known competing financial interests or personal relationships that could have appeared to influence the work reported in this paper.

Acknowledgements

Financial support for this project was provided by a grant from the U.S. National Science Foundation, Division of Chemistry (Grant No. NSF-CHE1953843). N.T. and R.P.P thank DGAPA-UNAM (Project Nos. IN101019 and IA100920) and Conacyt (Grant No. A1-S-9070) for partial financial support. Calculations were performed in the DGCTIC-UNAM Supercomputing Center (Project Nos. LANCAD-UNAM-DGTIC-051 and LANCAD-UNAM-DGTIC-368).

Appendix A. Supplementary material

Supplementary data to this article can be found online at https://doi.org/10.1016/j.jcat.2022.09.013.

References

[1] Z. Ma, F. Zaera, Heterogeneous catalysis by metals, in: R.A. Scott (Ed.) Encyclopedia of inorganic and bioinorganic chemistry, John Wiley & Sons, Ltd, Chichester, 2014, p. eibc0079.
[2] G.C. Bond, Metal-catalysed Reactions of Hydrocarbons, Springer, New York, 2005.
[3] D. Sanfilippo, P.N. Rylander, Hydrogenation and dehydrogenation, in: Ullmann's encyclopedia of industrial chemistry, Wiley-VCH Verlag GmbH & Co. KGaA, Weinheim, 2012, pp. 451–471.
[4] P. Gallezot, D. Richard, Selective hydrogenation of α, β-unsaturated aldehydes, Catal. Rev.-Sci. Technol. 40 (1998) 81–126.
[5] P. Claus, Selective hydrogenation of α, β-unsaturated aldehydes and other C=O and C=C bonds containing compounds, Top. Catal. 5 (1998) 51–62.
[6] M.S. Ide, B. Hao, M. Neurock, R.J. Davis, Mechanistic insights on the hydrogenation of α, β-unsaturated ketones and aldehydes to unsaturated alcohols over metal catalysts, ACS Catal. 2 (2012) 671–683.
[7] Y. Yuan, S. Yao, M. Wang, S. Lou, N. Yan, Recent progress in chemoselective hydrogenation of α, β-unsaturated aldehyde to unsaturated alcohol over nanomaterials, Curr. Org. Chem. 17 (2013) 400–413.
[8] F. Zaera, The surface chemistry of metal-based hydrogenation catalysis, ACS Catal. 7 (2017) 4947–4967.
[9] M. Tamura, Y. Nakagawa, K. Tomishige, Recent developments of heterogeneous catalysts for selective hydrogenation of unsaturated carbonyl compounds to unsaturated alcohols, J. Jpn. Pet. Inst. 62 (2019) 106–119.
[10] X. Lan, T. Wang, Highly selective catalysts for the hydrogenation of unsaturated aldehydes: a review, ACS Catal. 10 (2020) 2764–2790.
[11] X. Wang, X. Liang, P. Geng, Q. Li, Recent advances in selective hydrogenation of cinnamaldehyde over supported metal-based catalysts, ACS Catal. 10 (2020) 2395–2412.
[12] M. Johansson, O. Lytken, I. Chorkendorff, The sticking probability for H_2 on some transition metals at a hydrogen pressure of 1 bar, J. Chem. Phys. 128 (2008) 034706.
[13] L. Álvarez-Falcón, F. Viñes, A. Notario-Estévez, F. Illas, On the hydrogen adsorption and dissociation on Cu surfaces and nanorows, Surf. Sci. 646 (2016) 221–229.
[14] B. Chen, F. Zaera, Hydrogenation of cinnamaldehyde on Cu(110) single-crystal surfaces, J. Phys. Chem. C 125 (2021) 14709–14717.
[15] C.P. O'Brien, J.B. Miller, B.D. Morreale, A.J. Gellman, The kinetics of H_2–D_2 exchange over Pd, Cu, and PdCu surfaces, J. Phys. Chem. C 115 (2011) 24221–24230.
[16] G. Gumuslu, P. Kondratyuk, J.R. Boes, B. Morreale, J.B. Miller, J.R. Kitchin, A.J. Gellman, Correlation of electronic structure with catalytic activity: H_2–D_2 exchange across Cu_xPd_{1-x} composition space, ACS Catal. 5 (2015) 3137–3147.
[17] J. Han, J. Lu, M. Wang, Y. Wang, F. Wang, Single atom alloy preparation and applications in heterogeneous catalysis, Chin. J. Chem. 37 (2019) 977–988.
[18] R.T. Hannagan, G. Giannakakis, M. Flytzani-Stephanopoulos, E.C.H. Sykes, Single-atom alloy catalysis, Chem. Rev. 120 (2020) 12044–12088.
[19] M. Luneau, J.S. Lim, D.A. Patel, E.C.H. Sykes, C.M. Friend, P. Sautet, Guidelines to achieving high selectivity for the hydrogenation of α, β-unsaturated aldehydes with bimetallic and dilute alloy catalysts: a review, Chem. Rev. 120 (2020) 12834–12872.
[20] E.C.H. Sykes, P. Christopher, Recent advances in single-atom catalysts and single-atom alloys: opportunities for exploring the uncharted phase space in-between, Curr. Opin. Chem. Eng. 29 (2020) 67–73.
[21] F. Zaera, Designing sites in heterogeneous catalysis: are we reaching selectivities competitive with those of homogeneous catalysts?, Chem Rev. 122 (2022) 8594–8757.
[22] M.B. Boucher, B. Zugic, G. Cladaras, J. Kammert, M.D. Marcinkowski, T.J. Lawton, E.C.H. Sykes, M. Flytzani-Stephanopoulos, Single atom alloy surface analogs in $Pd_{0.18}Cu_{15}$ nanoparticles for selective hydrogenation reactions, Phys. Chem. Chem. Phys. 15 (2013) 12187–12196.
[23] F.R. Lucci, J. Liu, M.D. Marcinkowski, M. Yang, L.F. Allard, M. Flytzani-Stephanopoulos, E.C.H. Sykes, Selective hydrogenation of 1,3-butadiene on platinum–copper alloys at the single-atom limit, Nat. Commun. 6 (2015) 8550.

[24] G.X. Pei, X.Y. Liu, X. Yang, L. Zhang, A. Wang, L. Li, H. Wang, X. Wang, T. Zhang, Performance of Cu-alloyed Pd single-atom catalyst for semihydrogenation of acetylene under simulated front-end conditions, ACS Catal. 7 (2017) 1491–1500.
[25] M. Luneau, T. Shirman, A.C. Foucher, K. Duanmu, D.M.A. Verbart, P. Sautet, E.A. Stach, J. Aizenberg, R.J. Madix, C.M. Friend, Achieving high selectivity for alkyne hydrogenation at high conversions with compositionally optimized PdAu nanoparticle catalysts in raspberry colloid-templated SiO_2, ACS Catal. (2019) 441–450.
[26] Y. Cao, B. Chen, J. Guerrero-Sánchez, I. Lee, X. Zhou, N. Takeuchi, F. Zaera, Controlling selectivity in unsaturated aldehyde hydrogenation using single-site alloy catalysts, ACS Catal. 9 (2019) 9150–9157.
[27] Y. Cao, J. Guerrero-Sańchez, I. Lee, X. Zhou, N. Takeuchi, F. Zaera, Kinetic study of the hydrogenation of unsaturated aldehydes promoted by $CuPt_x$/SBA-15 single-atom alloy (SAA) catalysts, ACS Catal. 10 (2020) 3431–3443.
[28] F.R. Lucci, M.D. Marcinkowski, T.J. Lawton, E.C.H. Sykes, H_2 activation and spillover on catalytically relevant Pt–Cu single atom alloys, J. Phys. Chem. C 119 (2015) 24351–24357.
[29] M.T. Darby, M. Stamatakis, A. Michaelides, E.C.H. Sykes, Lonely atoms with special gifts: breaking linear scaling relationships in heterogeneous catalysis with single-atom alloys, J. Phys. Chem. Lett. 9 (2018) 5636–5646.
[30] G. Giannakakis, M. Flytzani-Stephanopoulos, E.C.H. Sykes, Single-atom alloys as a reductionist approach to the rational design of heterogeneous catalysts, Acc. Chem. Res. 52 (2019) 237–247.
[31] M.T. Darby, R. Réocreux, E.C.H. Sykes, A. Michaelides, M. Stamatakis, Elucidating the stability and reactivity of surface intermediates on single-atom alloy catalysts, ACS Catal. 8 (2018) 5038–5050.
[32] H. Thirumalai, J.R. Kitchin, Investigating the reactivity of single atom alloys using density functional theory, Top. Catal. 61 (2018) 462–474.
[33] J. Schumann, Y. Bao, R.T. Hannagan, E.C.H. Sykes, M. Stamatakis, A. Michaelides, Periodic trends in adsorption energies around single-atom alloy active sites, J. Phys. Chem. Lett. 12 (2021) 10060–10067.
[34] J.P. Simonovis, A. Hunt, R.M. Palomino, S.D. Senanayake, I. Waluyo, Enhanced stability of Pt-Cu single-atom alloy catalysts: In situ characterization of the Pt/Cu(111) surface in an ambient pressure of CO, J. Phys. Chem. C 122 (2018) 4488–4495.
[35] K.G. Papanikolaou, M.T. Darby, M. Stamatakis, CO-induced aggregation and segregation of highly dilute alloys: a density functional theory study, J. Phys. Chem. C 123 (2019) 9128–9138.
[36] S. Liu, Z.-J. Zhao, C. Yang, S. Zha, K.M. Neyman, F. Studt, J. Gong, Adsorption preference determines segregation direction: a shortcut to more realistic surface models of alloy catalysts, ACS Catal. 9 (2019) 5011–5018.
[37] M.A. van Spronsen, K. Daunmu, C.R. O'Connor, T. Egle, H. Kersell, J. Oliver-Meseguer, M.B. Salmeron, R.J. Madix, P. Sautet, C.M. Friend, Dynamics of surface alloys: rearrangement of Pd/Ag(111) induced by CO and o_2, J. Phys. Chem. C 123 (2019) 8312–8323.
[38] J.P. Simonovis, A. Hunt, S.D. Senanayake, I. Waluyo, Subtle and reversible interactions of ambient pressure H_2 with Pt/Cu(111) single-atom alloy surfaces, Surf. Sci. 679 (2019) 207–213.
[39] M.T. Nayakasinghe, J. Guerrero-Sánchez, N. Takeuchi, F. Zaera, Adsorption of crotonaldehyde on metal surfaces: Cu vs Pt, J. Chem. Phys. 154 (2021) 104701.
[40] B. Chen, R. Ponce, J. Guerrero-Sánchez, N. Takeuchi, F. Zaera, Cinnamaldehyde adsorption and thermal decomposition on copper surfaces, J. Vac. Sci. Technol., A 39 (2021) 053205.
[41] J. Simonovis, A. Tillekaratne, F. Zaera, The role of carbonaceous deposits in hydrogenation catalysis revisited, J. Phys. Chem. C 121 (2017) 2285–2293.
[42] A. Tilekaratne, J.P. Simonovis, M.F. López Fagúndez, M. Ebrahimi, F. Zaera, Operando studies of the catalytic hydrogenation of ethylene on Pt(111) single crystal surfaces, ACS Catal. 2 (2012) 2259–2268.
[43] A. Loaiza, M. Xu, F. Zaera, On the mechanism of the H-D exchange reaction in ethane over platinum catalysts, J. Catal. 159 (1996) 127–139.
[44] F. Zaera, H. Hoffmann, Detection of chemisorbed methyl and methylene groups: surface chemistry of methyl iodide on Pt(111), J. Phys. Chem. 95 (1991) 6297–6303.
[45] R. Morales, F. Zaera, Thermal chemistry of 1-methyl-1-cyclopentene and methylene cyclopentane on Pt(111) surfaces: evidence for double-bond isomerization, J. Phys. Chem. B 110 (2006) 9650–9659.
[46] F. Zaera, Infrared and molecular beam studies of chemical reactions on solid surfaces, Int. Rev. Phys. Chem. 21 (2002) 433–471.
[47] F. Zaera, New advances in the use of infrared absorption spectroscopy for the characterization of heterogeneous catalytic reactions, Chem. Soc. Rev. 43 (2014) 7624–7663.
[48] Y. Yao, J. Guerrero-Sánchez, N. Takeuchi, F. Zaera, Coadsorption of formic acid and hydrazine on Cu(110) single-crystal surfaces, J. Phys. Chem. C 123 (2019) 7584–7593.
[49] B. Chen, X. Qin, C. Lien, M. Bouman, M. Konh, Y. Duan, A.V. Teplyakov, F. Zaera, Thermal chemistry of metal organic compounds adsorbed on oxide surfaces, Organometallics 39 (2020) 928–940.
[50] Q. Ma, H. Guo, R.G. Gordon, F. Zaera, Uptake of copper acetamidinate ALD precursors on nickel surfaces, Chem. Mater. 22 (2010) 352–359.
[51] Q. Ma, F. Zaera, Thermal chemistry of the Cu-KI5 atomic layer deposition precursor on a copper surface, J. Vac. Sci. Technol., A 33 (2015) 01A108.
[52] F.M. Chua, Y. Kuk, P.J. Silverman, Oxygen chemisorption on Cu(110): an atomic view by scanning tunneling microscopy, Phys. Rev. Lett. 63 (1989) 386–389.
[53] R. Feidenhans'l, F. Grey, R.L. Johnson, S.G.J. Mochrie, J. Bohr, M. Nielsen, Oxygen chemisorption on Cu(110): a structural determination by x-ray diffraction, Phys. Rev. B 41 (1990) 5420–5423.
[54] Y. Yao, F. Zaera, Adsorption and thermal chemistry of formic acid on clean and oxygen-predosed Cu(110) single-crystal surfaces revisited, Surf. Sci. 646 (2016) 37–44.
[55] J. Wilson, H. Guo, R. Morales, E. Podgornov, I. Lee, F. Zaera, Kinetic measurements of hydrocarbon conversion reactions on model metal surfaces, Phys. Chem. Chem. Phys. 9 (2007) 3830–3852.
[56] A. Tillekaratne, J.P. Simonovis, F. Zaera, Ethylene hydrogenation catalysis on Pt (111) single-crystal surfaces studied by using mass spectrometry and in situ infrared absorption spectroscopy, Surf. Sci. 652 (2016) 134–141.
[57] Y. Dong, M. Ebrahimi, A. Tillekaratne, J.P. Simonovis, F. Zaera, Hydrogenation vs. H-D isotope scrambling during the conversion of ethylene with hydrogen/deuterium catalyzed by platinum under single-collision conditions, Phys. Chem. Chem. Phys. 18 (2016) 19248–19258.
[58] G. Kresse, J. Furthmüller, Efficient iterative schemes for ab initio total-energy calculations using a plane-wave basis set, Phys. Rev. B 54 (1996) 11169–11186.
[59] P.E. Blöchl, Projector augmented-wave method, Phys. Rev. B 50 (1994) 17953–17979.
[60] J.P. Perdew, K. Burke, M. Ernzerhof, Generalized gradient approximation made simple, Phys. Rev. Lett. 77 (1996) 3865–3868.
[61] S. Grimme, J. Antony, S. Ehrlich, H. Krieg, A consistent and accurate ab initio parametrization of density functional dispersion correction (DFT-d) for the 94 elements H-Pu, J. Chem. Phys. 132 (2010) 154104.
[62] G. Henkelman, B.P. Uberuaga, H. Jónsson, A climbing image nudged elastic band method for finding saddle points and minimum energy paths, J. Chem. Phys. 113 (2000) 9901–9904.
[63] G. Henkelman, H. Jónsson, Improved tangent estimate in the nudged elastic band method for finding minimum energy paths and saddle points, J. Chem. Phys. 113 (2000) 9978–9985.
[64] R.G. Greenler, Infrared study of adsorbed molecules on metal surfaces by reflection techniques, J. Chem. Phys. 44 (1966) 310–315.
[65] E.M. Stuve, R.J. Madix, Use of the π-σ parameter for characterization of rehybridization upon adsorption on metal surfaces, J. Phys. Chem. 89 (1985) 3183–3185.
[66] F. Zaera, Key unanswered questions about the mechanism of olefin hydrogenation catalysis by transition-metal surfaces: a surface-science perspective, Phys. Chem. Chem. Phys. 15 (2013) 11988–12003.
[67] S. Fujii, N. Osaka, M. Akita, K. Itoh, Infrared reflection absorption spectroscopic study on the adsorption structures of acrolein on an evaporated silver film, J. Phys. Chem. 99 (1995) 6994–7001.
[68] J.C. de Jesús, F. Zaera, Adsorption and thermal chemistry of acrolein and crotonaldehyde on Pt(111) surfaces, Surf. Sci. 430 (1999) 99–115.
[69] P.A. Redhead, Thermal desorption of gases, Vacuum 12 (1962) 203–211.
[70] D.L.S. Nieskens, A.P. van Bavel, J.W. Niemantsverdriet, The analysis of temperature programmed desorption experiments of systems with lateral interactions; implications of the compensation effect, Surf. Sci. 546 (2003) 159–169.
[71] F. Zaera, Kinetics on model systems, in: J. Reedijk, K. Poeppelmeier (Eds.), Comprehensive Inorganic Chemistry II, Elsevier, Oxford, UK, 2013, pp. 39–74.
[72] P. Rylander, Catalytic Hydrogenation Over Platinum Metals, Academic Press, New York, 1967.
[73] F. Zaera, G.A. Somorjai, Hydrogenation of ethylene over platinum (111) single-crystal surfaces, J. Am. Chem. Soc. 106 (1984) 2288–2293.
[74] F. Zaera, On the mechanism for the hydrogenation of olefins on transition-metal surfaces: the chemistry of ethylene on Pt(111), Langmuir 12 (1996) 88–94.
[75] Y. Dong, M. Ebrahimi, A. Tillekaratne, F. Zaera, Direct addition mechanism during the catalytic hydrogenation of olefins over platinum surfaces, J. Phys. Chem. Lett. 7 (2016) 2439–2443.
[76] F. Bournel, C. Laffon, P. Parent, G. Tourillon, Adsorption of some substituted ethylene molecules on Pt(111) at 95 k. II. A FT-RAIRS study, Surf. Sci. 359 (1996) 10–16.
[77] J.C. de Jesús, F. Zaera, Double-bond activation in unsaturated aldehydes: Conversion of acrolein to propene and ketene on Pt(111) surfaces, J. Mol. Catal. A: Chem. 138 (1999) 237–240.
[78] D.A. Esan, Y. Ren, X. Feng, M. Trenary, Adsorption and hydrogenation of acrolein on Ru(001), J. Phys. Chem. C 121 (2017) 4384–4392.
[79] K.-H. Dostert, C.P. O'Brien, F. Mirabella, F. Ivars-Barcelo, S. Schauermann, Adsorption of acrolein, propanal, and allyl alcohol on Pd(111): a combined infrared reflection-absorption spectroscopy and temperature programmed desorption study, Phys. Chem. Chem. Phys. 18 (2016) 13960–13973.
[80] K.-H. Dostert, C.P. O'Brien, F. Mirabella, F. Ivars-Barceló, S. Attia, E. Spadafora, S. Schauermann, H.-J. Freund, Selective partial hydrogenation of acrolein on Pd: a mechanistic study, ACS Catal. 7 (2017) 5523–5533.
[81] M. Muir, D.L. Molina, A. Islam, M.K. Abdel-Rahman, M. Trenary, Adsorption properties of acrolein, propanal, 2-propenol, and 1-propanol on Ag(111), Phys. Chem. Chem. Phys. 22 (2020) 25011–25020.
[82] M. Akita, N. Osaka, K. Itoh, Infra-red reflection absorption spectroscopic study on adsorption structures of acrolein on polycrystalline gold and Au(111) surfaces under ultra-high vacuum conditions, Surf. Sci. 405 (1998) 172–181.
[83] I.E. Wachs, R.J. Madix, The oxidation of ethanol on copper(110) and silver(110) catalysts, Appl. Surf. Sci. 1 (1978) 303–328.
[84] Y. Dong, F. Zaera, Selectivity in hydrogenation catalysis with unsaturated aldehydes: parallel versus sequential steps, J. Phys. Chem. Lett. 9 (2018) 1301–1306.